Proc. Nat. Acad. Sci. USA
Vol. 69, No. 3, pp. 561–565, March 1972

Photoelectron Microscopy: A New Approach to Mapping Organic and Biological Surfaces

(photoionization/photoemission/fluorescence microscopy/membranes)

O. H. GRIFFITH, G. H. LESCH, G. F. REMPFER*, G. B. BIRRELL, C. A. BURKE, D. W. SCHLOSSER, M. H. MALLON, G. B. LEE, R. G. STAFFORD, P. C. JOST, AND T. B. MARRIOTT

Institute of Molecular Biology and Department of Chemistry, University of Oregon, Eugene, Ore. 97403; and *Department of Physics, Portland State University, Portland, Oregon 97207

Communicated by Virgil Boekelheide, December 20, 1971

ABSTRACT **A general method of imaging organic and biological surfaces based on the photoelectric effect is reported. For the experiments, a photoelectron emission microscope was constructed. It is an ultrahigh vacuum instrument using electrostatic electron lenses, microchannel plate image intensifier, cold stage, hydrogen excitation source, and magnesium fluoride optics. The organic surfaces examined were grid patterns of acridine orange, fluorescein, and benzo(a)pyrene on a Butvar surface. A biological sample, sectioned rat epididymis, was also imaged by the new photoelectron microscope. Good contrast was obtained in these initial low magnification experiments. These data demonstrate the feasibility of mapping biological surfaces according to differences in ionization potentials of exposed molecules. A number of technical difficulties, such as the intensity of the excitation source, must be solved before high resolution experiments are practical. However, it is probable that this approach can be useful, even at low magnifications, in determination of the properties of organic and biological surfaces.**

Spectroscopic labeling techniques are becoming increasingly useful in studies of membranes and other biological surfaces. Labeling or tagging with organic dye molecules has long been recognized as a useful approach (1). The techniques are, of course, becoming more refined and the useful region of the electromagnetic spectrum has been greatly extended. The common techniques now include fluorescence (2, 3), optical absorption (3), electron spin resonance (3, 4), and nuclear magnetic resonance spectroscopy (3, 5). All of these techniques can yield information regarding molecular motion and orientation of molecules, and the polarity of specific binding sites. However, these spectroscopic methods do not determine the positions of the labels or distinguish between surface and bulk properties of the specimen. This is especially troublesome when dealing with biological surfaces (e.g., cell surfaces, nerve endings, and membranes of organelles). Understanding mechanisms of drug action, cell adhesion, membrane structure, immunological responses, and loss of contact inhibition in malignant cells require a knowledge of the relative positions, environments, and population densities of binding sites on the surface. *It is clear that new microscopic techniques are needed that can be combined with existing spectroscopic methods in studies of biological surfaces.* It was to develop new microscopic techniques that we began several years ago to examine the photoelectric effect of organic and biological surfaces.

A typical experiment is depicted in Fig. 1. The specimen is placed in a vacuum chamber and is then subjected to ultraviolet light. If the energy of the light source ($h\nu$) is sufficiently high, the sample surface can emit electrons (photoionize) as well as fluoresce. This *intrinsic* photoionization depends on the ionization potentials of various functional groups on or very near the surface. The process for individual molecules is described by the Einstein equation, $h\nu = I_n + E_n$, where I_n is the nth molecular ionization potential and E_n is the excess kinetic energy of the ejected electron (small corrections for solid effects have been omitted). In Fig. 1*A*, for example, the energy of the incident light is slightly greater than the lowest ionization potential of molecule X but is not of sufficient energy to photoionize Y or Z. The photoelectrons will originate from molecules of type X and, if the electrons are accelerated and imaged on a phosphor screen, a measure of the distribution of these molecules will be obtained. Furthermore, if intrinsic photoionization is weak or if more information is desired, it should be possible to bind photoionization labels (P) to specific sites and produce *extrinsic* photoionization (see Fig. 1*B*). We refer to images formed by intrinsic or extrinsic photoionization from organic molecules as *photoelectron microscopy*. Photoelectron microscopy is a different technique from conventional transmission electron microscopy or scanning electron microscopy. In conventional or scanning electron microscopy a beam of electrons is first accelerated and then passed through (or scattered from) the fixed, stained, or metal-coated sample. In photoelectron microscopy, however, the biological surface itself emits the electrons under the action of ultraviolet light. This approach bears a close relationship to fluorescence microscopy performed with incident ultraviolet light. One major difference is that electrons are emitted instead of photons, and resolution limitations are related to the wavelength of the electrons and not to the wavelength of visible light. A second important difference is that the properties of the surface are distinguished from those of the bulk specimen. Thus, photoelectron microscopy can be viewed as a logical extension of fluorescence microscopy to the study of biological surfaces with electron optics.

The imaging of electrons produced by the action of ultraviolet light is not new. It is a type of emission microscopy and, together with thermionic emission, represents one of the

Abbreviation: PEM, photoelectron microscope.

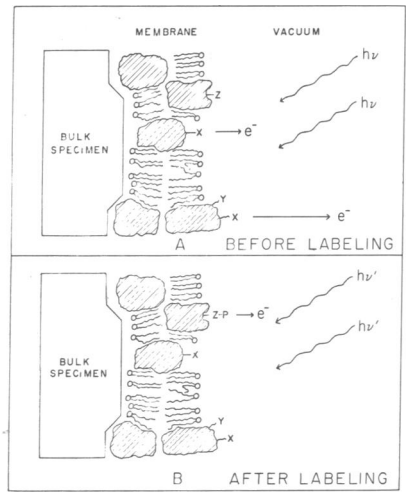

FIG. 1. The photoionization of electrons from a hypothetical biological surface. The top diagram illustrates intrinsic photoionization from certain functional groups (X) on the biological surface. In the bottom diagram, the site Z has been labeled with a photoionizing probe P and the energy of the incident light has been adjusted from $h\nu$ to $h\nu'$. After labeling, photoelectrons originate predominately from sites Z–P (*extrinsic photoionization*).

earliest developments in electron microscopy. In 1932, Brüche and Johannson (6) and Knoll *et al.* (7) described images produced by thermionic emission from a hot cathode. Shortly thereafter, Brüche (8) and Mahl and Pohl (9) constructed instruments to image photoelectrons. The early applications included forming images of hot tungsten filaments, barium and strontium oxide-coated cathodes, and examining the structure of metallic surfaces (7–10). Emission microscopy has developed slowly but it is still a relatively obscure and specialized technique when compared to conventional transmission electron microscopy or scanning electron microscopy. Recently, Möllenstedt, Lenz, and Wegmann and others (11) have made noteworthy contributions to the development of emission microscopes and have reported a number of interesting applications in metallurgy and related fields.

Also relevant to our work are measurements of photoionization yields and kinetic energy (E_n) distributions of the photoelectrons. The experimental apparatus usually consists of a monochromatic light source, a vacuum chamber containing the solid or gaseous sample and, more recently, an electron energy analyzer. Organic solid surfaces have been studied primarily by investigators interested in applying the theories and techniques of solid state physics to crystalline organic semiconductors (12). A few photoelectric yield measurements have also been made on biomolecules (13). However, the majority of recent work involves an energy analyzer and is called photoelectron spectroscopy (PES or UPS) (14) or electron spectroscopy for chemical analysis (ESCA or XPS) (15), depending on whether an ultraviolet lamp or x-ray source is used. Photoelectron spectroscopy provides information on the valence shell electronic structure of molecules in the gas phase, whereas electron spectroscopy for chemical analysis provides information also on the ionized inner core electrons and is most often used in studies of solid surfaces. Of these two techniques, photoelectron spectroscopy is much more closely related to the experiments depicted in Fig. 1. The success of photoelectron microscopy will depend, in part, on the wealth of ionization potential and angular distribution data provided in the elegant studies by photoelectron spectroscopy of organic compounds by Turner and others (14).

In this paper, we report the completion of the first steps of our program to map organic and biological surfaces by the photoelectric effect. A photoelectron microscope designed for imaging organic and biological samples has been constructed. The initial data are presented below along with a discussion of the feasibility and limitations of this approach.

MATERIALS AND METHODS

Photoelectron Microscope. A simplified diagram of the photoelectron microscope (PEM) is given in Fig. 2. Light from a McPherson model 630 Hinteregger hydrogen lamp is reflected from a magnesium fluoride coated aluminum mirror onto the sample. The sample mount (cathode) is held at -10 kV to -30 kV by a model 5030-4 Sorenson power supply. Electrons ejected from the sample are accelerated toward the anode, focused, and passed through a small hole in the mirror, projector lens, and onto the image intensifier and phosphor screen. The PEM is an oil-free, stainless steel ultrahigh vacuum system pumped by one Varian 500 liter/sec ion pump and two Varian molecular sieve roughing pumps. The base pressure is in the 10^{-9}–10^{-10} torr range. Varian Conflat flanges and copper gaskets were used in constructing the microscope and the only elastomer seal is located inside the Varian 15.24-cm (6-inch) gate valve. The electron lenses are of the electrostatic unipotential type (16). Lens properties were determined experimentally by the ray-tracing method of Spangenberg and Field (17). The PEM is equipped with two electrostatic lens systems, one for low (about × 10–200) and the other for high (about × 200–8000) magnification ranges. The low

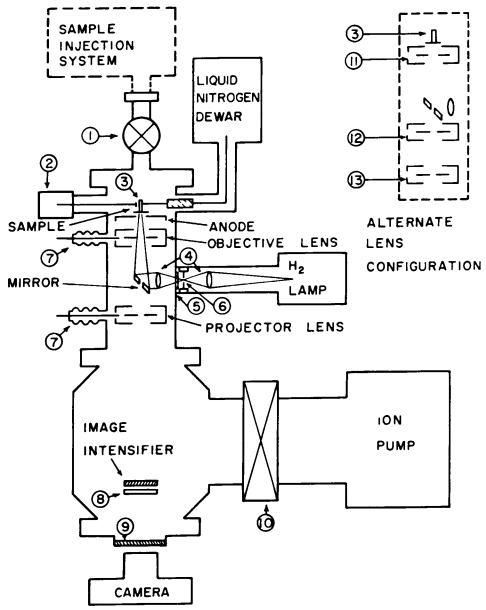

FIG. 2. Schematic diagram of the photoelectron microscope. (*1*) Metal-sealed straight-through valve; (*2*) stage translators; (*3*) sample rod; (*4*) magnesium fluoride lenses; (*5*) magnesium fluoride window; (*6*) aperture; (*7*) high voltage ceramic feedthroughs; (*8*) aluminized phosphor screen; (*9*) glass viewing port; (*10*) 15.24-cm (6-inch) Viton-sealed gate valve; (*11*) short focal length objective lens; (*12*) intermediate lens; and (*13*) projector lens of the second electron lens system.

magnification lenses shown inside the PEM in Fig. 2 were used to record all data of this paper. There is, at present, no objective aperture in this two-lens system. The image intensifier is a Varian microchannel plate 2.54-cm (1-inch) in diameter. The liquid nitrogen dewar (Linde model CR-10), magnesium fluoride lenses (Muffoletto Optical Co.), and Polaroid camera are standard commercial products.

Organic and Biological Samples. Acridine orange and fluorescein were purchased from Matheson, Coleman and Bell Co. Benzo(a)pyrene was obtained from Sigma Co. and Butvar-98 (polyvinyl butyral) was purchased from Monsanto Co. All chemicals were used without further purification. The standard PEM sample mount is a gold plated copper rod, 6.35 mm in diameter, 2.54-cm long and has a protruding ring near the upper end to position the rod in the sample stage assembly. The lower end (sample end) of the rod is routinely dipped into a 0.5% solution of Butvar in chloroform. The resulting Butvar coating suppresses photoemission from the gold surface. Organic grid patterns were prepared by sublimation of a small amount of acridine orange, fluorescein, or benzo(a)pyrene through a 100 × 400 mesh copper EM grid (Perforated Products), 3.05 mm in diameter (Ernest F. Fullam, Inc.), held against the Butvar-coated sample rod. The copper grid was then removed leaving a well defined test pattern.

Rat epididymis specimens were dissected from mature Sprague-Dawley rats. Some tissue samples were fixed 1 hr in 4% glutaraldehyde in Millonig's phosphate buffer (pH 7.2) and washed a minimum of 2 hr by several changes of the same buffer. Fixed or fresh tissue was sectioned by a Harris-International cryostat. The 12-μm thick frozen sections were mounted on Butvar-coated sample rods and were air dried at room temperature before examination in the PEM.

RESULTS AND DISCUSSION

Organic Patterns on an Organic Substrate. There are several questions concerning the feasibility of imaging organic and biological surfaces. Some of these are (*a*) Is the photoelectron current sufficient to produce an image? (*b*) Assuming that the photoelectron current is sufficient, will contrast be observed? (*c*) Will photochemical reactions degrade the surface before an image can be recorded? (*d*) Is sample conductivity an insurmountable obstacle? The answers will depend, of course, on magnification, instrument resolution, sample temperature, and type of specimen. In order to determine partial answers to these questions, we began with simple patterns of organic compounds. The three molecules chosen were acridine orange (I), fluorescein (II) and benzo(a)pyrene (III).

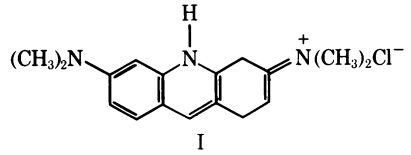

I

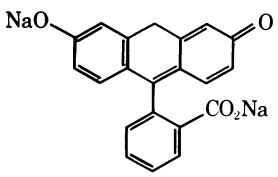

II

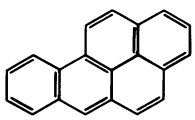

III

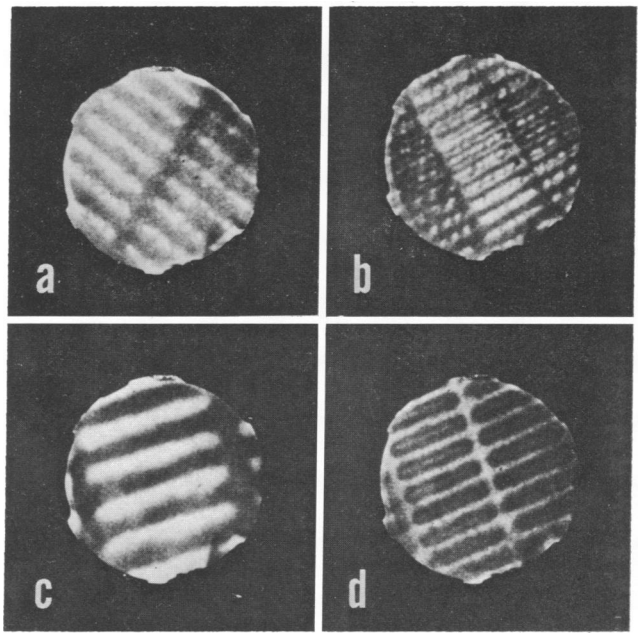

FIG. 3. Photoelectron micrographs of organic grid patterns. *a*, acridine orange on a Butvar surface, ×55. *b*, fluorescein on Butvar, ×35. *c*, benzo(a)pyrene on Butvar, ×80. *d*, a control sample consisting of a pattern of magnesium fluoride on gold, ×50. The film exposure times (*f*/2 lens) were 1/10, 1/5, 1/2, and 1/5 sec, respectively. The field of view is determined by the microchannel plate holder (note the tabs visible in all micrographs). The sample stage temperature was about 80–100°K in all four experiments.

Acridine orange was selected because it is widely used in fluorescence microscopy (e.g., binding to DNA- or RNA-rich regions) (18). Fluorescein is frequently conjugated to antibody proteins in fluorescent immunochemical investigations (2). The third molecule chosen (III) is a chemical carcinogen of current interest (19).

Thin parallel strips 20 × 215 μm were prepared by subliming each compound through a 100 × 400 mesh copper grid onto the Butvar-coated sample support. Immediately after switching on the hydrogen lamp, grid patterns appeared on the phosphor screen. Typical micrographs are given in Fig. 3. These patterns disappeared as soon as the lamp was turned off or when a small magnet was placed next to the microscope column. This establishes the fact that the grid patterns are formed by electrons emitted by the organic sample, under the action of ultraviolet light.

It is clear from micrographs *a*, *b*, and *c* of Fig. 3 that the photoelectron current and contrast from organic samples are quite adequate for these initial, low magnification experiments. For comparison, Fig. 3*d* is the image of a sample prepared by evaporation of magnesium fluoride through a 100 × 400 mesh grid onto a gold surface. Note that the contrast is reversed. The photoelectrons originate predominately from the gold surface and not from the strips of magnesium fluoride. Fig. 3*d* provides two important observations. First, photoionization is the dominant process rather than photoinduced field emission (i.e., the image appears to depend strongly on ionization potentials and not solely on surface contour). Secondly, image brightness in the case of organic samples is comparable to that observed for the gold pattern, which suggests that conductivity of the organic samples is

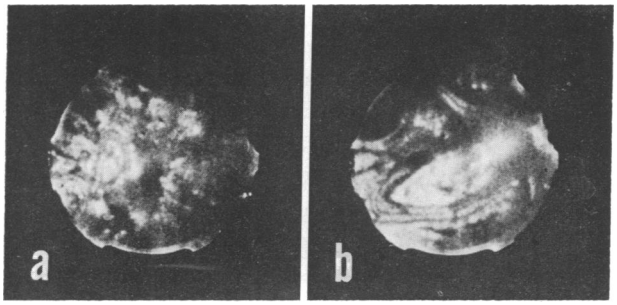

FIG. 4. Photoelectron micrographs of sectioned rat epididymis. *a*, unfixed tissue section, ×19. (*f*/2 lens; exposure time 1/2 sec). The near-horizontal boundary near the top of the micrograph represents the edge of the biological sample. *b*, glutaraldehyde-fixed tissue section, ×30. (*f*/2 lens; exposure time 1.0 sec). The temperature of the sample stage was about 80–100°K.

not as serious a problem as we originally thought. Surface photochemistry is more difficult to evaluate. Some damage almost certainly occurs, even at 80–100°K. However, the images photographed in Fig. 3 were stable, and no changes in contrast were observed over a period of several hours.

A Biological Sample: Rat Epididymis. Rat epididymis was chosen as an initial biological sample because the well-characterized morphology can be examined at low magnifications. Thin sections of fixed epididymis from a mature rat were placed in the PEM and cooled to 80–100°K to minimize photochemical damage. Immediately after starting the hydrogen lamp, an image appeared on the phosphor screen. The image disappeared when the lamp was switched off. These images were deflected by the presence of magnetic or electrostatic fields, and there is no doubt that they were produced by electrons ejected from the specimen or the Butvar-coated sample rod. Typical images are shown in Fig. 4. Some variation in intensity with time was noted and may be caused by sample charging. The photoelectron micrographs of Fig. 4 represent preliminary work and no detailed study of contrast as a function of sample preparation or lamp excitation spectrum has been attempted. Certain features do, however, appear to be present in all images photographed thus far. The cross sections of the tubules are easily recognized by their regular circular outlines (see Fig. 4). In Fig. 4*b* there appears to be some fine detail in the epithelial and connective tissue regions. The ducts are filled with masses of spermatozoa, as confirmed by photographs of the same sample viewed with reflected light microscopy. In the PEM, these sperm masses show up as bright areas. Contrast is remarkably good considering that the samples are unstained. The contrast is almost certainly caused by differences in ionization potentials of various regions of the specimen. This, then, is an example of intrinsic photoionization from a biological specimen. We cannot at this point exclude the possibility that variations in sample thickness or density contribute to image contrast, or that some photoelectrons may originate from the Butvar-coated sample rod. However, these secondary effects could hardly account for the basic morphological features observed in the photoelectron micrographs of Fig. 4.

Theoretical Resolution Limits. The final resolution obtainable in the photoelectron microscope will depend on a number of factors that can be divided into two categories; instrumental characteristics and sample characteristics. The first category includes properties of the accelerating field and the lenses that affect the imaging of the electron radiation, i.e., spherical aberration, chromatic aberration, astigmatism, and alignment of optical components. The second category involves such considerations as the distribution of velocities and directions of the emitted electrons, and the resolution inherent in the beam of photoemitted electrons as affected by the wavelengths of the electrons as they leave the emitting surface. To some extent, these two categories are related; one must consider the spread in electron trajectories, for instance, in calculating resolution limitations due to spherical aberration.

We have performed calculations on these various resolution factors but space limitations permit only a brief mention of the salient points. Detailed calculations will be published later [see also Grivet (16)]. The most important errors arise from the spherical aberration of the accelerating field (r_a), the diffraction limitation due to the wave nature of the electron (r_d), and the spherical error of the objective lens (r_1), where the r values denote the corresponding radii of circles of least confusion. For example, $r_a = (0.6a)(\sin \alpha_{om})(1 - \cos \alpha_{om})(\epsilon_0/eV)$ where a is the cathode–anode separation, α_{om} is the angular aperture of emission, ϵ_0 is the energy of the emitted electrons, e is the charge of an electron, and V is the accelerating voltage. The combined effect of the errors gives an overall resolution limit $r = (r^2_1 + r^2_a + r^2_d)^{1/2}$. For the high magnification three lens system of Fig. 2, $a = 3$ mm, $V = 3 \times 10^4$ volts, $f = 7$ mm, and $C_s = 20$, where f is the focal length of the objective lens and C_s is a dimensionless aberration coefficient of the objective lens that enters into the calculation of r_1. In Table 1, the values of ϵ_0 that minimize r for this system are given along with the resulting resolution limits for several values of the limiting angle of emission.

Table 1 shows that for small values of the photoelectron energy the spherical error (r_1) of the objective lens is negligible compared with that of the accelerating field and diffraction limitations, while as ϵ_0 increases the lens error becomes relatively more important. The final resolution range is from 44 Å to 26 Å. However, the figures in Table 1 were calculated under the assumption that the angular aperture is uniformly filled with electron rays from the specimen. If instead, strong spurs in the distribution were present at a certain angle to the normal, as they would be in the case of repeated fine sample detail, the resolution of this detail could be much better than that indicated in Table 1. *We conclude that the theoretical resolution of the photoelectron microscope is sufficient to allow mapping of biological surfaces to at least 40 Å resolution, and the resolution limit does not depend on the thickness of the specimen.* Since 40 Å is in the range of typical protein dimensions, photoelectron microscopy has the potential of determining the distribution of specific proteins in biological membranes.

Prognosis. The major instrumental limitation at present is the ultraviolet light source. In order to achieve high magnifications, better light sources in the 150–240 nm (1500–2400 Å) region and improved image intensifiers are essential. There is, of course, no guarantee that the organic and biological surfaces will be sufficiently stable even at low temperature to produce an image when subjected to high-intensity illumination. This problem is reminiscent of fluorescence microscopy, where high intensity sources and low-image brightness present a challenge to the experimenter. Other technical difficulties

TABLE 1. *Optimum energy of the emitted electrons and corresponding resolution limits for various limiting angles of emission*

α_{om}	90°	60°	45°	30°	5.7° (0.1 rad)
ϵ_0 (ev)	0.042	0.078	0.15	0.37	11
r_1 (Å)	2.9	5	7	9.5	13
r_a (Å)	25	20	16	12	4
r_d (Å)	36	30	28	24	22
r (Å)	44	37	33	29	26

include proper choice of photoelectron labels or stains (based on ionization potentials, conductivity, and angular distribution of photoelectrons), unstained specimen conductivity, the effects of electric fields on ionization potentials, and a detailed analysis of the origin of contrast. Recent developments in light sources and image intensifiers introduce an optimistic note. For example, Hodgson (20) and Waynant *et al.* (21) have developed hydrogen lasers [about 160 nm (1600 Å)] that could, with some development, serve directly as a light source or indirectly as the excitation source for vacuum-ultraviolet tunable dye lasers. With the present light source, the PEM images of organic and biological samples are encouraging from the point of view of brightness, contrast, and sample stability. It is significant that such useful fluorescent labels as acridine orange and fluorescein have attractive photoionization yields. Finally, it should be noted that photoelectron microscopy can be useful even at very low magnifications. Image contrast in PEM is based largely on photoionization potentials of molecules on or near the surface rather than optical absorption of the entire specimen. Thus, the information content is different from that of optical micrographs, and optically transparent surfaces (e.g., some unstained biological membranes) may well have interesting photoelectric properties.

We thank G. D. Kuhl for advice and help in preparation of the biological samples and H. M. Howard for his expert light microscopy. We acknowledge the contributions of J. Bonfonti, H. G. Cathery, B. Crasemann, R. Dam, Jr., A. C. Fabergé, D. Frisbie, M. Gurevitch, C. V. Muffoletto, J. Rennie, E. Schabtach, G. Turner, and the staffs of Elektros, The Night Vision Laboratory (Fort Belvoir), Optics Technology, Tektronix, Varian, and Wilbanks Inc. This research was supported in large part by U.S. Public Health Service grant CA11695-02 from the National Cancer Institute. Early instrument construction was initiated under the Young Faculty Grant Program of E.I. du Pont de Nemours and Co. We also thank Varian for some instrumentation. A recent Teacher–Scholar grant from the Camille and Henry Dreyfus Foundation greatly accelerated the project. Finally, this work benefited from general facilities provided by a Health Sciences Advancement Award to the University of Oregon.

1. Reiner, L. (1930) *Science* **72,** 483–484; Coons, A. H., Creech, H. J. & Jones, R. N. (1941) *Proc. Soc. Exp. Biol. and Med.* **47,** 200–202; Weber, G. (1952) *Biochem. J.* **51,** 155–167.
2. Stryer, L. (1968) *Science* **162,** 526–533; Nairn, R. C. (1969) *Fluorescent Protein Tracing* (Williams and Wilkins Co., Baltimore).
3. Chance, B., Lee, C. & Blasie, J. K., eds., *Probes of Structure and Function of Macromolecules and Membranes* (Academic Press, New York), Vols. I and II.
4. McConnell, H. M. & McFarland, B. G. (1970) *Quart. Rev. Biophys.* **3,** 91–136; Jost, P., Waggoner, A. S. & Griffith, O. H. (1971) in *Structure and Function of Biological Membranes,* ed. Rothfield, L. I. (Academic Press, New York), chap. 3.
5. Roberts, G. E. K. & Jardetsky, O. (1970) *Advan. in Protein Chem.* **24,** 447–545; Cohn, M. & Reuben, J. (1971) *Accounts. Chem. Res.* **4,** 214–222.
6. Brüche, E. & Johannson, H. (1932) *Naturwissenschaften* **20,** 353–358.
7. Knoll, M., Houtermans, F. G., & Schulze, W. (1932) *Z. Phys.* **78,** 340–362.
8. Brüche, E. (1933) *Z. Physik.* **86,** 448–450.
9. Mahl, H. & Pohl, J. (1935) *Z. Tech. Phys.* **16,** 219.
10. Burton, E. F. & Kohl, W. H. (1942) *The Electron Microscope* (Reinhold, New York), chap. 14 and 15.
11. Möllenstedt, G. & Lenz, F. (1963) *Advan. Electronics and Electron Physics* **18,** 251–329; Engel, W. (1966) *Sixth Intern. Congr. for Electron Microscopy (Maruzen Co., Tokyo),* pp. 217–218; Turner, G. & Bauer, E. (1966) *Sixth Intern. Congr. for Electron Microscopy (Maruzen Co., Tokyo),* pp. 163–164; Wegmann, L. (1966) *Sixth Intern. Congr. for Electron Microscopy (Maruzen Co., Tokyo),* pp. 283–284; Wegmann, L. (1968) *Prakt. Metallogr.* **5,** 241-263; Wegmann, L. (1969) in *Handbuch der Zerstörungsfreien Materialprüfng,* ed. Müller, E. A. W. (Oldenbourg-Verlag, München), R 31, p. 1.
12. Gutmann, F. & Lyons, L. E. (1967) *Organic Semiconductors* (John Wiley, New York).
13. Setlow, R. B. (1960) *Radiat Res. Suppl.* **2,** 276–289; Berger, K. U. (1969) *Z. Naturforsch. B* **B24,** 722–728.
14. Turner, D. W. (1970) *Annu. Rev. Phys. Chem.* **21,** 107–128; Worley, S. D. (1971) *Chem. Rev.* **71,** 295–314.
15. Siegbahn, K. *et al.* (1967) *ESCA: Atomic, Molecular and Solid State Structure Studied by Means of Electron Spectroscopy* (Almqvist and Wiksells, Uppsala).
16. Grivet, P. (1965) *Electron Optics* (Pergamon Press, Oxford).
17. Spangenberg, K. & Field, L. (1942) *Proc. Institute Radio Engineers* **30,** 138–144.
18. Thompson, S. W. (1966) *Selected Histochemical and Histopathological Methods* (C. C Thomas, Springfield, Ill.).
19. Daudel, P. & Daudel, R. (1966) *Chemical Carcinogenesis and Molecular Biology* (Wiley-Interscience, New York); Cavalieri, E. & Calvin, M. (1971) *Proc. Nat. Acad. Sci. USA* **68,** 1251–1253.
20. Hodgson, R. T. (1970) *Phys. Rev. Lett.* **25,** 494–497.
21. Waynant, R. W., Shipman, J. D., Jr., Elton, R. C. & Ali, A. W. (1971) *Proc. of the Institute of Electrical and Electronics Engineers,* **59** 679–684.